Formation drivers and photochemical effects of $ClNO_2$ in a coastal city of Southeast China

Gaojie Chen[1,4,5], Xiaolong Fan[1,4], Haichao Wang[2*], Yee Jun Tham[3], Ziyi Lin[1,4,5], Xiaoting Ji[1,4,5], Lingling Xu[1,4], Baoye Hu[6], Jinsheng Chen[1,4*]

[1]Center for Excellence in Regional Atmospheric Environment, Institute of Urban Environment, Chinese Academy of Sciences, Xiamen 361021, China

[2]School of Atmospheric Sciences, Sun Yat-sen University, Zhuhai 519082, China

[3]School of Marine Sciences, Sun Yat-sen University, Zhuhai 519082, China

[4]Fujian Key Laboratory of Atmospheric Ozone Pollution Prevention, Institute of Urban Environment, Chinese Academy of Sciences, Xiamen 361021, China

[5]University of Chinese Academy of Sciences, Beijing 100049, China

[6]Minnan Normal University, Zhangzhou 363000, China

*Correspondence to: Jinsheng Chen (jschen@iue.ac.cn); Haichao Wang (wanghch27@mail.sysu.edu.cn).

Abstract. Nitryl chloride ($ClNO_2$) is an important precursor of chlorine (Cl) radical, significantly affecting ozone (O_3) formation and photochemical oxidation. However, the key drivers of $ClNO_2$ production are not fully understood. In this study, the field observations of $ClNO_2$ and related parameters were conducted in a coastal city of Southeast China during the autumn of 2022, combining with machine learning and model simulations to elucidate its key influencing factors and atmospheric impacts. Elevated concentrations of $ClNO_2$ (> 500 ppt) were notably observed during nighttime in late autumn, accompanied by increased levels of dinitrogen pentoxide (N_2O_5) and nitrate (NO_3^-). Nighttime concentrations of $ClNO_2$ peaked at 3.4 ppb, while its daytime levels remained significant, reaching up to 100 ppt and sustaining at approximately 40 ppt at noon. Machine learning and field observations identified nighttime N_2O_5 heterogeneous uptake as the predominant pathway for $ClNO_2$ production, whereas NO_3^- photolysis may contribute to its daytime generation. Additionally, ambient temperature (T) and relative humidity (RH) emerged as primary meteorological factors affecting $ClNO_2$ formation, mainly through their effects on thermal equilibrium and N_2O_5 hydrolysis processes, respectively. Ultraviolet (UV) radiation was found to play a dual role in $ClNO_2$ concentrations around noon. Box model simulations showed that under high $ClNO_2$ conditions, the rates of alkane oxidation by Cl radical in the early morning exceeded those by OH radical. Consequently, VOC oxidation by Cl radical contributed ~ 19% to RO_x production rates, thereby significantly impacting O_3 formation and atmospheric oxidation capacity. This research enriched the understanding of $ClNO_2$ generation and loss pathways, providing valuable insights for the regulation of photochemical pollution in coastal regions.

1 Introduction

Chlorine (Cl) radical, as an important atmospheric oxidant, can react with volatile organic compounds (VOCs) to affect RO_x (including OH, HO_2, and RO_2) radicals and ozone (O_3) formation (Yi et al., 2023), thereby perturbing atmospheric chemical components and air quality (Peng et al., 2021; Li et al., 2020). The reaction rates between Cl radical and some alkanes are several orders of magnitude faster than those involving OH radical (Atkinson et al., 2006). Furthermore, the related studies indicated that the production rates of Cl radical in the early morning could significantly exceed the production rates of OH radical formed via O_3 photolysis (Phillips et al., 2012; Tham et al., 2016), thereby enhancing the atmospheric oxidation capacity.

Nitryl chloride ($ClNO_2$) is one of the major Cl radical precursors in the tropospheric atmosphere (Thornton et al., 2010; Xue et al., 2015; Liu et al., 2017). It is mainly generated by the heterogeneous uptake of dinitrogen pentoxide (N_2O_5) on chloride-containing aerosols (Finlayson-Pitts et al., 1989; Thornton et al., 2010), among which N_2O_5 is produced through the equilibrium reaction with nitrogen dioxide (NO_2) and nitrate (NO_3) radical. Since Osthoff et al. (2008) firstly detected over 1 ppb of $ClNO_2$ in the urban outflows

of America (Osthoff et al., 2008), significant production of $ClNO_2$ has been widely observed in the polluted coastal and inland areas with abundant anthropogenic emissions and chloride sources, with concentrations ranging from tens of ppt to several ppb (Riedel et al., 2012; Mielke et al., 2013; Mielke et al., 2011; Phillips et al., 2012; Bannan et al., 2015; Wang et al., 2016; Xia et al., 2020; Xia et al., 2021; Yun et al., 2018; Wang et al., 2022; Li et al., 2023). For the diurnal profile of $ClNO_2$, its concentrations generally peaked and accumulated at midnight, then rapidly decreased to low levels due to strong photolysis after sunrise (Ma et al., 2023; Mielke et al., 2011; Xia et al., 2020). However, elevated daytime concentrations of $ClNO_2$ have been observed in field studies, mainly attributed to reduced photolysis rates under heavy cloud or fog cover, as well as contributions from horizontal and vertical transport (Tham et al., 2016; Xia et al., 2021; Jeong et al., 2019; Mielke et al., 2013; Bannan et al., 2015). Notably, the recent laboratory research demonstrated that nitrate (NO_3^-) photolysis can generate $ClNO_2$ alongside Cl_2 (Dalton et al., 2023), yet this mechanism has not been confirmed under real atmospheric conditions.

At present, the observation studies of $ClNO_2$ focused on investigating its influencing factors, such as the N_2O_5 uptake coefficient and the production yield of $ClNO_2$ (Thornton et al., 2003; Tham et al., 2018). The field and laboratory studies have indicated that $ClNO_2$ production was mainly affected by ambient temperature (T), relative humidity (RH), and particle components (e g., chloride (Cl^-), NO_3^-, and liquid water content) (Bertram and Thornton, 2009; Wang et al., 2023; Wang et al., 2020). In addition to influencing factors, the photochemical effects of $ClNO_2$ photolysis have been extensively evaluated (Xue et al., 2015; Xia et al., 2021; Tham et al., 2016). Cl radical released by $ClNO_2$ photolysis will oxidize VOCs to promote the formation of RO_2 radical and O_3, greatly compensating for the underestimation of RO_2 radical and O_3 generation in model simulations (Peng et al., 2021; Ma et al., 2023). The field measurements of $ClNO_2$ have been conducted in different atmospheric environments, while the key drivers of $ClNO_2$ chemistry were still not well recognized. Moreover, it is pertinent to explore whether there are additional and unrecognized sources of $ClNO_2$ beyond its heterogeneous generation from N_2O_5.

In this study, the comprehensive measurements of $ClNO_2$ and related parameters were conducted in a coastal city of Southeast China during the autumn of 2022. Field observations, combined with a machine learning model, were used to reveal the key driving factors of $ClNO_2$ formation. Furthermore, we further investigated the potential mechanisms driving daytime $ClNO_2$ generation. Additionally, we also assessed the photochemical impacts of $ClNO_2$ based on a box model. Overall, this study underscored the important role of NO_3^- in the $ClNO_2$ chemistry.

2 Materials and methods

2.1 Field Measurements

The intensive field measurements of $ClNO_2$, related precursors, and meteorological parameters from October 9th to December 5th, 2022 were performed at an urban site (Institute of Urban Environment,

Chinese Academy of Sciences) in a coastal city (Xiamen) of Southeast China (Fig. S1). Here, $ClNO_2$, N_2O_5, gaseous pollutants (volatile organic compounds (VOCs), NO_x, SO_2, CO, and O_3), aerosol mass concentrations, ionic components, size distribution, and meteorological factors were simultaneously detected. Meanwhile, an iodide-adduct time-of-flight chemical ionization mass spectrometer (I^--ToF-CIMS) was used to measure $ClNO_2$ and N_2O_5. The principles and settings of I^--ToF-CIMS were similar with previous studies (Ma et al., 2023; Yan et al., 2023). Detailed descriptions of this observation site and instruments have been provided in previous work (Chen et al., 2024; Hu et al., 2022), Text S1, and Table S1. For the calibrations of $ClNO_2$ and N_2O_5, $ClNO_2$ was produced by passing Cl_2 (6 ppm in N_2) through a moist mixture of sodium nitrite ($NaNO_2$) and sodium chloride (NaCl) (Thaler et al., 2011; Wang et al., 2022), and N_2O_5 was synthesized by the reactions of O_3 and excessive NO_2 (Tham et al., 2016; Wang et al., 2016). The dependences of $ClNO_2$ and N_2O_5 sensitivities on relative humidity are presented in Fig. S2. The uncertainties of the $ClNO_2$ and N_2O_5 measurements were estimated to be ~15 and 12 %, respectively. The details of $ClNO_2$ and N_2O_5 calibrations and uncertainty analysis are displayed in Text S2.

2.2 Machine Learning model

Here, the extreme gradient boosting (XGBoost) model coupling with the Shapely additive explanations (SHAP) model (the XGBoost-SHAP model) was used to identify the key influencing factors of $ClNO_2$ formation. Meanwhile, the XGBoost model was applied to establish the predictive model of $ClNO_2$ based on the observed data of gaseous precursors and meteorological factors; the SHAP model was employed to evaluate the importance of each feature affecting the simulated concentrations of $ClNO_2$. The SHAP model is an interpretability tool designed to analyze the contributions of individual features to model predictions. It employs an additive explanatory framework that considers all features as contributors, drawing inspiration from cooperative game theory. For each predicted instance, SHAP assigns a Shapley value, representing the cumulative contribution of each feature. Positive SHAP values indicate that a feature increases the model's predicted outcome, signifying a positive contribution. Conversely, negative SHAP values suggest that the feature reduces the predicted value, reflecting a negative contribution. The absolute value of the SHAP score reflects the magnitude of the contribution, regardless of direction, offering insight into the overall importance of the feature. The true value, on the other hand, reveals the direction of the contribution (positive or negative), facilitating a clearer understanding of the relationship between the feature and the prediction. Besides, the partial dependence plot (PDP) analysis offers a visual representation of the marginal effect that the factors have on the model's predicted outcome. It is based on the principle of stabilizing the values of non-target features, and systematically altered the target feature's values according to the model's algorithmic framework to derive the predicted values.

$ClNO_2$ concentrations served as the dependent variable, with trace gases (SO_2, CO, NO_2, NO, O_3, and N_2O_5), $PM_{2.5}$ and its inorganic compositions (NO_3^-, SO_4^{2-}, NH_4^+, and Cl^-), and meteorological parameters (T, RH, UV, WS, WD, and BLH) acting as independent variables. The simulated $ClNO_2$ concentrations by the

XGBoost model were highly similar with the observed values (R^2=0.91), indicating the good performance of the XGBoost model (Fig. S3). Detailed introductions and settings of the XGBoost-SHAP model are provided in Text S3.

2.3 The box model

The observation-based model (OBM) was utilized to assess the impacts of $ClNO_2$ on photochemically atmospheric oxidation. As delineated in earlier studies (Xue et al., 2015; Tham et al., 2016; Xia et al., 2021; Peng et al., 2021; Peng et al., 2022), the Master Chemical Mechanism (MCM, version 3.3.1) was adopted, and established chlorine chemistry mechanisms have been integrated. The Tropospheric Ultraviolet and Visible Radiation (TUV) model was used to calculate $ClNO_2$ photolysis rates ($JClNO_2$) under clear-sky conditions. The simulated $JClNO_2$ values were then scaled based on field-measured JNO_2 values. A thorough exposition of the box model configuration can be found in our previous publications (Liu et al., 2022b; Liu et al., 2022a) and Text S4. Observation data, including $ClNO_2$, VOCs, HCHO, HONO, CO, O_3, NO, NO_2, SO_2, along with meteorological factors as constraint were input into the box model at an hourly resolution (Table S2). Two scenarios were examined: one representing observation-average conditions from October 9th to December 5th, the other reflecting a high $ClNO_2$ case observed on November 28th.

This study focused on elucidating the influence of $ClNO_2$ on the formation of RO_x radical and O_3. The O_3 production rate minus the O_3 loss rate was used to calculate the net O_3 production rate (Eq. S1-3). The AOC is calculated by the sum of the rates of CH_4, CO, and VOCs oxidized by atmospheric oxidants (O_3, OH, Cl, and NO_3 radical) (Eq. S4) (Xue et al., 2015; Yi et al., 2023). Both scenarios were evaluated with and without including $ClNO_2$ inputs to assess its impacts on these processes.

3 Results and discussion

3.1 Overview of observations

Fig. 1 displays the time series of $ClNO_2$, N_2O_5, and related parameters including O_3, NO_x, $PM_{2.5}$, Cl^-, NO_3^-, and meteorological parameters during the autumn observation period. Our observation shows a decline in T and UV values from October to November, with average RH values increasing from ~ 60% in October to ~ 70% in November (excluding rainy days). During the entire measurement period, $ClNO_2$ concentrations exhibited significant variability, with elevated levels (> 500 ppt) frequently observed in late autumn, particularly after November 10th. The elevation of $ClNO_2$ concentrations coincided with increased levels of N_2O_5 and NO_3^- during late autumn. The concentrations of $ClNO_2$ at our study site reached several ppb, compared with previous field measurements conducted at urban, suburban, rural, background, and mountain sites (Table S3), indicating its widespread presence in diverse atmospheric environments. The highest concentrations of $ClNO_2$ were detected during the night of November 27th, with a maximum hourly average of 3.4 ppb. Peak concentrations of N_2O_5 and NO_3^- were also observed on that night (Fig. 1). On the evening of November 27th, N_2O_5 concentrations rapidly decreased after 7 p.m., while $ClNO_2$ and NO_3^-

concentrations significantly increased, reflecting fast N_2O_5 heterogeneous hydrolysis and effective formation of $ClNO_2$. Notably, on the following day (November 28th) (Fig. 2a), $ClNO_2$ concentrations sustained above 100 ppt around noon, partially related with weaken UV values (~ 14 $W \cdot m^{-2}$) under heavy fog and cloud cover, with the RH values of ~ 70% at that time. Similar research in California has shown $ClNO_2$ concentrations exceeding 100 ppt after sunrise 4 hours due to reduced photolysis (Mielke et al., 2013).

The average diurnal changes of $ClNO_2$ and related parameters during the entire measurement campaign are depicted in Fig. 2b. As expected, $ClNO_2$ exhibited a distinct diurnal variation, peaking and accumulating after sunset and decreasing in the early morning. However, $ClNO_2$ concentrations remained ~ 40 ppt around noon, different with some studies that $ClNO_2$ concentrations decreased to near the detection limit around midday (Wang et al., 2022; Niu et al., 2022). Similar observation in North China declared $ClNO_2$ concentrations above 60 ppt in the afternoon (Liu et al., 2017). Previous studies have indicated that abundant $ClNO_2$ may be transported from upper atmosphere or air mass, contributing to the elevated $ClNO_2$ concentrations in the early morning (Tham et al., 2016; Xia et al., 2021; Jeong et al., 2019). However, the explanations for the concentrations of $ClNO_2$ around noon remained elusive.

To evaluate the contribution of the heterogeneous N_2O_5 uptake to daytime $ClNO_2$ levels, we calculated $ClNO_2$ production using a box model, considering (1) the contribution of heterogeneous N_2O_5 uptake to $ClNO_2$ production, and (2) $ClNO_2$ loss via photolysis, aerosol uptake, and reaction with OH· (Text S5 and S6). We used a $\gamma(N_2O_5)$ value of 0.06, a $\phi(ClNO_2)$ value of 1.0, and a $\gamma(ClNO_2)$ value of 0.006 in our calculations, which represent upper-end estimates based on previous field studies (Mcduffie et al., 2018a; Mcduffie et al., 2018b; Tham et al., 2016). However, as shown in Fig. 3, the simulated daytime $ClNO_2$ concentrations were lower than the observed values. Therefore, we believe that the observed daytime $ClNO_2$ levels, particularly around noon, cannot be adequately explained by heterogeneous N_2O_5 uptake alone, suggesting the presence of additional sources contributing to the formation of daytime $ClNO_2$.

3.2 Key drivers of $ClNO_2$ formation

The XGBoost-SHAP model was employed to investigate the major drivers of $ClNO_2$ production during the whole observation period. The average absolute SHAP value of each feature was ranked to determine the key drivers of $ClNO_2$ formation, with larger SHAP values suggesting greater contributions (Fig. 4a). Additionally, features with positive SHAP values (depicted as red points) indicate that higher values of those features positively affect $ClNO_2$ concentrations, and vice versa (Fig. 4b). Overall, N_2O_5, NO_3^-, T, RH, and UV were the most important features affecting $ClNO_2$ concentrations. Notably, these factors exhibited varied behaviors between daytime and nighttime periods.

In our study, N_2O_5 was identified as the most important influencing factor, consistent with its role in $ClNO_2$ formation through heterogeneous uptake processes (Thornton et al., 2010; Finlayson-Pitts et al., 1989). After sunset, $ClNO_2$ concentrations markedly increased due to active nighttime N_2O_5 chemistry, while this heterogeneous uptake process was hindered after sunrise as N_2O_5 concentrations decreased

significantly (Fig. 1) (Niu et al., 2022; Wang et al., 2020; Tan et al., 2022). Indeed, the concentrations of $ClNO_2$ were evidently increased when N_2O_5 concentrations exceeded ~13 ppt, predominantly during the nighttime (Fig. 5a). Conversely, in Northern Europe, the $ClNO_2$ concentrations were mainly controlled by O_3 and NO_2, rather than by the heterogeneous uptake of N_2O_5 (Sommariva et al., 2018). In Heshan of South China, chloride and $PM_{2.5}$ were the major factors affecting $ClNO_2$ formation (Wang et al., 2022). Differently, the relative importance of NO_3^- derived from the XGBoost-SHAP result indicated that elevated $ClNO_2$ concentrations were associated with high concentrations of NO_3^- besides N_2O_5. According to Fig. 5b, high NO_3^- concentrations (> 3.7 $\mu g \cdot m^{-3}$) are accompanied by the elevation of $ClNO_2$, especially its concentrations reaching 6.2 $\mu g \cdot m^{-3}$. Previous studies suggested that increased concentrations of NO_3^- decreased $\gamma(N_2O_5)$, which would limit the production of $ClNO_2$ (Wahner et al., 1998; Mentel et al., 1999; Bertram and Thornton, 2009). As depicted in Fig. S4, the dependence of $\gamma(N_2O_5)$ on NO_3^- concentrations follows the nitrate suppression effect. Therefore, the importance of nighttime NO_3^- for $ClNO_2$ levels is that they are co-products from the processes of N_2O_5 heterogeneous uptake. As shown in Fig. 1, compared to low NO_3^- conditions, $ClNO_2$ production was enhanced in high NO_3^- conditions. Especially in late autumn, increased aerosol abundances and N_2O_5 levels enhanced N_2O_5 uptake further promoting $ClNO_2$ and NO_3^- production. Considering the limited contribution of N_2O_5 hydrolysis to daytime NO_3^- levels (Yan et al., 2023; Zang et al., 2022; Chen et al., 2020), the impact of high NO_3^- concentrations on daytime $ClNO_2$ concentrations warrants further analysis.

The simulated concentrations of $ClNO_2$, based on the XGBoost-SHAP model, were significantly elevated when NO_3^- concentrations were higher than 3.7 $\mu g \cdot m^{-3}$ (Fig. 5b). Consequently, the average daily concentrations of NO_3^- were classified as high (> 3.7 $\mu g \cdot m^{-3}$) and low (< 3.7 $\mu g \cdot m^{-3}$) to further elucidate the impacts of NO_3^- on the formation of $ClNO_2$. Fig. 6 presents the diurnal variations in the relative importance of factors based on the SHAP values under high and low NO_3^- concentrations. Unexpectedly, daytime NO_3^- was the dominant influencing factors for daytime $ClNO_2$ (Fig. 6a). High concentrations of daytime NO_3^- positively affected the daytime concentrations of $ClNO_2$, independent of N_2O_5 uptake processes. As depicted in Fig. 6a, daytime N_2O_5 did not promote the elevation of daytime $ClNO_2$. Negative SHAP values for N_2O_5 during the daytime indicate that the contribution of N_2O_5 chemistry to daytime $ClNO_2$ levels was limited. Therefore, it is very likely that high concentrations of daytime NO_3^- participated in daytime $ClNO_2$ production. A recent study suggested that nitrate photolysis produced $ClNO_2$ in addition to Cl_2 (Dalton et al., 2023), while it has been not verified by field observations. Fig. 7 shows that daytime $ClNO_2$ concentrations correlated well (R=0.62) with the product of a proxy of NO_3^- photolysis ($NO_3^- \times JNO_2 \times S_a$) on aerosol surfaces, implying that the photolysis of NO_3^- likely resulted in the daytime formation of $ClNO_2$ at our study site. Furthermore, high concentrations of NO_3^- and Cl^-, along with large values of S_a (Fig. 7a, b, c and Fig. S5) in the daytime accelerated NO_3^- photolysis, promoting the formation of $ClNO_2$, while $ClNO_2$ concentrations exhibited a weak correlation with JNO_2. It should be emphasized that the weak correlation

between JNO_2 and $ClNO_2$ concentrations does not deny the potential contribution of nitrate photolysis, which could be explained by the fact that $ClNO_2$ concentrations are affected by both its production and loss processes. Specifically, photolysis rates exert dual effects on daytime $ClNO_2$ concentrations: positive effects through photochemical production pathways and negative effects through direct $ClNO_2$ photolytic loss. Given the short daytime lifetime of $ClNO_2$, we calculated the missing $ClNO_2$ production rate (production rate minus loss rate) to assess the contributions from unknown sources (Text S6). The production rates of unknown sources showed a good correlation with JNO_2 (R=0.41) (Fig. S6), indicating that photochemical processes may enhance $ClNO_2$ production. Notably, the strong correlation between the observed concentrations of $ClNO_2$ and the NO_3^- photolysis proxy ($NO_3^-\times JNO_2\times S_a$) has revealed the possibility of the contribution of NO_3^- photolysis to the unknown daytime $ClNO_2$ source.

In term of meteorological factors, UV, T, and RH were the major influencing factors. The photolysis was the most important sink of $ClNO_2$ in the daytime, leading to a rapid reduction in $ClNO_2$ concentrations, particularly in the early morning (Fig. 5e and Fig. 6). However, it is crucial to understand the dual role of photolysis intensity in determining daytime $ClNO_2$ levels. As mentioned before, photolysis can contribute to the generation of $ClNO_2$ by promoting NO_3^- photolysis, while also causing the rapid decomposition of $ClNO_2$. As reported in California (Mielke et al., 2013), reduced photolysis rates even increased daytime $ClNO_2$ levels by decreasing $ClNO_2$ loss through photolysis. The impact of ambient temperature on $ClNO_2$ was probably reflected in its thermal equilibrium with N_2O_5. Elevated daytime ambient temperature suppressed the formation of N_2O_5, resulting in low N_2O_5 concentrations, which further limited the contribution of heterogeneous N_2O_5 uptake to daytime $ClNO_2$ generation (Fig. 5c and Fig. 6). During the whole observation period from October to November, the drop in ambient temperature facilitated $ClNO_2$ production by decreasing the thermal decomposition process. Increased RH values provided favorable conditions for the nighttime N_2O_5 hydrolysis reactions, thereby affecting $ClNO_2$ production (Fig. 5d and Fig. 6), while high RH (> 80%) also weakened the generation of $ClNO_2$. Notably, Cl^- was not the most important factors of $ClNO_2$ formation at our study site (Fig. 4), likely attributed to the abundant chlorine source in coastal regions (Peng et al., 2022).

3.3 Impact of $ClNO_2$ photolysis on RO_x budget

The photochemical effects of $ClNO_2$ were evaluated under the observation-average condition and the high $ClNO_2$ case based on the box model. The largest Cl production rates (P(Cl)) contributed from $ClNO_2$ photolysis were 0.05 $ppb\cdot h^{-1}$ for the observation-average condition, which was lower than 0.19 $ppb\cdot h^{-1}$ for the high $ClNO_2$ case. The difference led to variable levels of atmospheric oxidation capacity induced by Cl radical. Cl radical released via the photolysis of $ClNO_2$ initiated the oxidation of VOCs. Among VOC groups (including alkanes, alkenes, alkynes, aromatics, and OVOCs), Cl radical primarily oxidized alkanes (~ 65.0%), followed by OVOCs (~ 12.7%) for both the observation-average condition and the high $ClNO_2$ case (Fig. 8a, b). The contributions of Cl radical and other atmospheric oxidants (including OH radical and

O_3) to daytime VOC oxidation were also compared (Fig. 8c, d and Table 1). In our study, the oxidation of alkanes by Cl radical for the observation-average condition were about 11.7%, which increased by 44.8% for the high $ClNO_2$ case, were higher than those in London (Bannan et al., 2015), Weybourne (Bannan et al., 2017), Boston (Rutherford et al., 1995), and LA (Fraser et al., 1997), lower than that in Hong Kong (Xue et al., 2015). It should be noticed that the rates of Cl radical reacting with alkanes even exceeded those of OH radical in the early morning for the high $ClNO_2$ case. The largest rates of alkanes oxidized by Cl radical were approximately twice as high as those of OH radical at 10 a.m. (Fig. 8e, f), highlighting that the photochemical effects of Cl radical released via $ClNO_2$ photolysis were particularly important for VOC oxidation during the morning hours at our study site.

The oxidation of VOCs by Cl radical further affects the generation of RO_x (OH + HO_2 + RO_2) radicals. The RO_x radical production rates for the high $ClNO_2$ case were evidently lower than that under the observation-average condition, primarily due to reduced photolysis rates on that day. However, the total RO_x radical production rates averagely increased by 23.8% with $ClNO_2$ photolysis for the high $ClNO_2$ case, higher than a 4.9% increase for the observation-average condition (Fig. S7). For the observation-average condition, O_3 (32.7%), HONO (31.7%), and OVOCs (21.6%) photolysis were the most significant contributors to RO_x radical production in the early morning (7-10 a.m.), with VOC oxidation by Cl radical contributing only 3.7% (Fig. 9a). However, for the high $ClNO_2$ case, VOC oxidation induced by Cl radical in the early morning accounted for 19.1% of RO_x radical production, which was higher than O_3 (7.4%) and HCHO (4.1%) photolysis, close to OVOCs (19.0%) photolysis (Fig. 9b). The contributions of $ClNO_2$ photolysis to the RO_x radical production rates in our study were larger than previous results observed in autumn of Heshan (Wang et al., 2022) and North China (Xia et al., 2021), similar with that in summer of Wangdu (Tham et al., 2016). Thus, the concentrations of OH, HO_2, and RO_2 radicals in the box model with $ClNO_2$ inputs averagely increased by 17.9%, 34.6%, and 54.3% for the high $ClNO_2$ case, higher than the increases of 3.7%, 7.1%, and 10.3% contributed from the observation-average conditions, respectively (Fig. S8). The uplift in the concentrations of RO_x radicals also accelerated the generation of O_3. The increase in the net O_3 production rates ($P(O_3)$) for the observation-average condition averagely reached 0.13 $ppb \cdot h^{-1}$ (15.8 %) in the daytime (Fig. 10a), while larger elevations in the net $P(O_3)$ were observed for the high $ClNO_2$ case (Fig. 10b), with a maximum of 0.64 $ppb \cdot h^{-1}$ (120 %) at 10 a.m. As a result, increased RO_x radical and O_3 greatly enhanced the atmospheric oxidation capacity (Fig. 10c, d), especially for the high $ClNO_2$ case (up to 65%).

Table 2 summarizes the impacts of $ClNO_2$ photolysis on RO_x radical and O_3 production in our study and previous observations around the world (Xia et al., 2021; Wang et al., 2022; Tham et al., 2016; Wang et al., 2016; Xue et al., 2015; Bannan et al., 2017; Jeong et al., 2019), indicating that the photochemical impacts of $ClNO_2$ were variable in different atmospheric environments. At our study site, the effects of $ClNO_2$ photolysis on RO_x radical production were important, especially in the early morning. The enhanced

RO_x radical production induced by $ClNO_2$ photolysis accelerated the chemical generation of O_3. Primary RO_x radical production rates (including O_3, HONO, HCHO, OVOCs, and $ClNO_2$) were considered as one of the most important parameters to O_3 formation (Lu et al., 2023). Therefore, the considerable contribution of $ClNO_2$ photolysis to primary RO_x radical production in the early morning may bring new challenges for O_3 alleviation.

Conclusions

In conclusion, we present two months of field measurements in the coastal area of Southern China during the autumn, coupled with machine learning and model simulations, providing new insights into $ClNO_2$ chemistry. Our observation shows the increase in the concentrations of $ClNO_2$ were accompanied by elevated concentrations of N_2O_5 and NO_3^-, low values of T and UV, and high values of RH. The nighttime heterogeneous uptake of N_2O_5 was identified as the major source of $ClNO_2$, while NO_3^- photolysis served as a potential daytime $ClNO_2$ source. Cl radical released by $ClNO_2$ photolysis after sunrise had important photochemical effects in the early morning. The photolysis of high $ClNO_2$ concentrations resulted in net O_3 production rates and atmospheric oxidation capacity levels increasing by 120% and 65%, respectively. Our results enhanced the understanding of $ClNO_2$ chemistry in coastal regions, calling for more observations and laboratory research to fully reveal its exact role in different atmospheric environments.

Data availability. Data are available upon request to Jinsheng Chen (jschen@iue.ac.cn).

Author contributions. JC provided funding support for field measurements, designed this study, and revised this manuscript. GC designed this study, analyzed the data, and wrote this manuscript. HW helped perform the calibrations and revised this manuscript. XF revised this manuscript. XF, HW, YT, ZL, XJ, LX, BH contributed to discussions of this manuscript.

Competing interests. The authors declare that they have no conflict of interest.

Acknowledgements. The authors acknowledge the National Natural Science Foundation of China, the Science and Technology Department of Fujian Province, Center for Excellence in Regional Atmospheric Environment Project, Xiamen Atmospheric Environment Observation and Research Station of Fujian Province, and Fujian Key Laboratory of Atmospheric Ozone Pollution Prevention (Institute of Urban Environment, Chinese Academy of Sciences).

Financial support. This work was funded by the National Natural Science Foundation of China (U22A20578, 42305102 & 42277091), the Science and Technology Department of Fujian Province

(2022L3025), the National Key Research and Development Program (2022YFC3700304), STS Plan Supporting Project of the Chinese Academy of Sciences in Fujian Province (2023T3013), Fujian Provincial Environmental Protection Science & Technology Plan Projects (2023R004), and Xiamen Atmospheric Environment Observation and Research Station of Fujian Province. Y.J.T. acknowledges the funding support from the Guangdong Basic and Applied Basic Research Foundation (2022A1515010852) and the Fundamental Research Funds for the Central Universities, Sun Yat-sen University (23hytd002).

References

Atkinson, R., Baulch, D. L., Cox, R. A., Crowley, J. N., Hampson, R. F., Hynes, R. G., Jenkin, M. E., Rossi, M. J., Troe, J., and Subcommittee, I.: Evaluated kinetic and photochemical data for atmospheric chemistry: Volume II – gas phase reactions of organic species, Atmos. Chem. Phys., 6, 3625-4055, https://doi.org/10.5194/acp-6-3625-2006, 2006.

Bannan, T. J., Bacak, A., Le Breton, M., Flynn, M., Ouyang, B., McLeod, M., Jones, R., Malkin, T. L., Whalley, L. K., Heard, D. E., Bandy, B., Khan, M. A. H., Shallcross, D. E., and Percival, C. J.: Ground and Airborne U.K. Measurements of Nitryl Chloride: An Investigation of the Role of Cl Atom Oxidation at Weybourne Atmospheric Observatory, J. Geophys. Res. Atmos., 122, 11,154-111,165, https://doi.org/10.1002/2017jd026624, 2017.

Bannan, T. J., Booth, A. M., Bacak, A., Muller, J. B. A., Leather, K. E., Le Breton, M., Jones, B., Young, D., Coe, H., Allan, J., Visser, S., Slowik, J. G., Furger, M., Prévôt, A. S. H., Lee, J., Dunmore, R. E., Hopkins, J. R., Hamilton, J. F., Lewis, A. C., Whalley, L. K., Sharp, T., Stone, D., Heard, D. E., Fleming, Z. L., Leigh, R., Shallcross, D. E., and Percival, C. J.: The first UK measurements of nitryl chloride using a chemical ionization mass spectrometer in central London in the summer of 2012, and an investigation of the role of Cl atom oxidation, J. Geophys. Res. Atmos., 120, 5638-5657, https://doi.org/10.1002/2014jd022629, 2015.

Bertram, T. and Thornton, J.: Toward a general parameterization of N_2O_5 reactivity on aqueous particles: the competing effects of particle liquid water, nitrate and chloride, Atmos. Chem. Phys., 9, 8351-8363, https://doi.org/10.5194/acp-9-8351-2009, 2009.

Chen, G., Ji, X., Chen, J., Xu, L., Hu, B., Lin, Z., Fan, X., Li, M., Hong, Y., and Chen, J.: Photochemical pollution during summertime in a coastal city of Southeast China: Ozone formation and influencing factors, Atmos. Res., 301, 107270, https://doi.org/10.1016/j.atmosres.2024.107270, 2024.

Chen, X., Wang, H., Lu, K., Li, C., Zhai, T., Tan, Z., Ma, X., Yang, X., Liu, Y., Chen, S., Dong, H., Li, X., Wu, Z., Hu, M., Zeng, L., and Zhang, Y.: Field Determination of Nitrate Formation Pathway in Winter Beijing, Environ. Sci. Technol., 54, 9243-9253, https://doi.org/10.1021/acs.est.0c00972, 2020.

Dalton, E. Z., Hoffmann, E. H., Schaefer, T., Tilgner, A., Herrmann, H., and Raff, J. D.: Daytime Atmospheric Halogen Cycling through Aqueous-Phase Oxygen Atom Chemistry, J. Am. Chem. Soc., 145, 15652-15657, https://doi.org/10.1021/jacs.3c03112, 2023.

Finlayson-Pitts, B. J., Ezell, M. J., and Pitts, J. N.: Formation of chemically active chlorine compounds by reactions of atmospheric NaCl particles with gaseous N_2O_5 and $ClONO_2$, Nature., 337, 241-244, https://doi.org/10.1038/337241a0, 1989.

Fraser, M. P., Cass, G. R., Simoneit, B. R., and Rasmussen, R.: Air quality model evaluation data for organics. 4. C2−C36 non-aromatic hydrocarbons, Environ. Sci. Technol., 31, 2356-2367, https://doi.org/10.1021/es960980g, 1997.

Hu, B., Duan, J., Hong, Y., Xu, L., Li, M., Bian, Y., Qin, M., Fang, W., Xie, P., and Chen, J.: Exploration of the atmospheric chemistry of nitrous acid in a coastal city of southeastern China: results from measurements across four seasons, Atmos. Chem. Phys., 22, 371-393, https://doi.org/10.5194/acp-22-371-2022, 2022.

Jeong, D., Seco, R., Gu, D., Lee, Y., Nault, B. A., Knote, C. J., McGee, T., Sullivan, J. T., Jimenez, J. L., Campuzano-Jost, P., Blake, D. R., Sanchez, D., Guenther, A. B., Tanner, D., Huey, L. G., Long, R., Anderson, B. E., Hall, S. R., Ullmann, K., Shin, H., Herndon, S. C., Lee, Y., Kim, D., Ahn, J., and Kim, S.: Integration of airborne and ground observations of nitryl chloride in the Seoul metropolitan area and the implications on regional oxidation capacity during KORUS-AQ 2016, Atmos. Chem. Phys., 19, 12779-12795, https://doi.org/10.5194/acp-19-12779-2019, 2019.

Li, F., Huang, D. D., Nie, W., Tham, Y. J., Lou, S., Li, Y., Tian, L., Liu, Y., Zhou, M., and Wang, H.: Observation of nitrogen oxide-influenced chlorine chemistry and source analysis of Cl_2 in the Yangtze River Delta, China, Atmos. Environ., 306, 119829, https://doi.org/10.1016/j.atmosenv.2023.119829, 2023.

Li, Q., Badia, A., Wang, T., Sarwar, G., Fu, X., Zhang, L., Zhang, Q., Fung, J., Cuevas, C. A., Wang, S., Zhou, B., and Saiz-Lopez, A.: Potential Effect of Halogens on Atmospheric Oxidation and Air Quality in China, J. Geophys. Res. Atmos., 125, e2019JD032058, https://doi.org/10.1029/2019JD032058, 2020.

Liu, T., Chen, G., Chen, J., Xu, L., Li, M., Hong, Y., Chen, Y., Ji, X., Yang, C., Chen, Y., Huang, W., Huang, Q., and Wang, H.: Seasonal characteristics of atmospheric peroxyacetyl nitrate (PAN) in a coastal city of Southeast China: Explanatory factors and photochemical effects, Atmos. Chem. Phys., 22, 4339-4353, https://doi.org/10.5194/acp-22-4339-2022, 2022a.

Liu, T., Hong, Y., Li, M., Xu, L., Chen, J., Bian, Y., Yang, C., Dan, Y., Zhang, Y., Xue, L., Zhao, M., Huang, Z., and Wang, H.: Atmospheric oxidation capacity and ozone pollution mechanism in a coastal city of southeastern China: analysis of a typical photochemical episode by an observation-based model, Atmos.

Chem. Phys., 22, 2173-2190, https://doi.org/10.5194/acp-22-2173-2022, 2022b.

Liu, X., Qu, H., Huey, L. G., Wang, Y., Sjostedt, S., Zeng, L., Lu, K., Wu, Y., Hu, M., Shao, M., Zhu, T., and Zhang, Y.: High Levels of Daytime Molecular Chlorine and Nitryl Chloride at a Rural Site on the North China Plain, Environ. Sci. Technol., 51, 9588-9595, https://doi.org/10.1021/acs.est.7b03039, 2017.

Lu, K., Zhou, H., Lee, J., Nelson, B., and Zhang, Y.: Ozone mitigations beyond the control of nitrogen oxides and volatile organic compounds, Sci Bull, 68, 1989-1992, https://doi.org/10.1016/j.scib.2023.07.051., 2023.

Ma, W., Chen, X., Xia, M., Liu, Y., Wang, Y., Zhang, Y., Zheng, F., Zhan, J., Hua, C., and Wang, Z.: Reactive Chlorine Species Advancing the Atmospheric Oxidation Capacities of Inland Urban Environments, Environ. Sci. Technol., 57, 14638-14647, https://doi.org/10.1021/acs.est.3c05169, 2023.

McDuffie, E. E., Fibiger, D. L., Dubé, W. P., Lopez Hilfiker, F., Lee, B. H., Jaeglé, L., Guo, H., Weber, R. J., Reeves, J. M., Weinheimer, A. J., Schroder, J. C., Campuzano-Jost, P., Jimenez, J. L., Dibb, J. E., Veres, P., Ebben, C., Sparks, T. L., Wooldridge, P. J., Cohen, R. C., Campos, T., Hall, S. R., Ullmann, K., Roberts, J. M., Thornton, J. A., and Brown, S. S.: $ClNO_2$ Yields From Aircraft Measurements During the 2015 WINTER Campaign and Critical Evaluation of the Current Parameterization, J. Geophys. Res. Atmos., 123, 12,994-913,015, https://doi.org/10.1029/2018JD029358, 2018a.

McDuffie, E. E., Fibiger, D. L., Dubé, W. P., Lopez-Hilfiker, F., Lee, B. H., Thornton, J. A., Shah, V., Jaeglé, L., Guo, H., Weber, R. J., Michael Reeves, J., Weinheimer, A. J., Schroder, J. C., Campuzano-Jost, P., Jimenez, J. L., Dibb, J. E., Veres, P., Ebben, C., Sparks, T. L., Wooldridge, P. J., Cohen, R. C., Hornbrook, R. S., Apel, E. C., Campos, T., Hall, S. R., Ullmann, K., and Brown, S. S.: Heterogeneous N_2O_5 Uptake During Winter: Aircraft Measurements During the 2015 WINTER Campaign and Critical Evaluation of Current Parameterizations, J. Geophys. Res. Atmos., 123, 4345-4372, https://doi.org/10.1002/2018JD028336, 2018b.

Mentel, T. F., Sohn, M., and Wahner, A. J. P. C. C. P.: Nitrate effect in the heterogeneous hydrolysis of dinitrogen pentoxide on aqueous aerosols, Phys. Chem. Chem. Phys., 1, 5451-5457, https://doi.org/10.1039/A905338g, 1999.

Mielke, L. H., Furgeson, A., and Osthoff, H. D.: Observation of $ClNO_2$ in a Mid-Continental Urban Environment, Environ. Sci. Technol., 45, 8889-8896, https://doi.org/10.1021/es201955u, 2011.

Mielke, L. H., Stutz, J., Tsai, C., Hurlock, S. C., Roberts, J. M., Veres, P. R., Froyd, K. D., Hayes, P. L., Cubison, M. J., Jimenez, J. L., Washenfelder, R. A., Young, C. J., Gilman, J. B., Gouw, J. A., Flynn, J. H., Grossberg, N., Lefer, B. L., Liu, J., Weber, R. J., and Osthoff, H. D.: Heterogeneous formation of nitryl

chloride and its role as a nocturnal NO*x* reservoir species during CalNex-LA 2010, J. Geophys. Res. Atmos., 118, 10,638-610,652, https://doi.org/10.1002/jgrd.50783, 2013.

Niu, Y.-B., Zhu, B., He, L.-Y., Wang, Z., Lin, X.-Y., Tang, M.-X., and Huang, X.-F.: Fast Nocturnal Heterogeneous Chemistry in a Coastal Background Atmosphere and Its Implications for Daytime Photochemistry, J. Geophys. Res. Atmos., 127, e2022JD036716, https://doi.org/10.1029/2022JD036716, 2022.

Osthoff, H. D., Roberts, J. M., Ravishankara, A. R., Williams, E. J., Lerner, B. M., Sommariva, R., Bates, T. S., Coffman, D., Quinn, P. K., Dibb, J. E., Stark, H., Burkholder, J. B., Talukdar, R. K., Meagher, J., Fehsenfeld, F. C., and Brown, S. S.: High levels of nitryl chloride in the polluted subtropical marine boundary layer, Nat. Geosci., 1, 324-328, https://doi.org/10.1038/ngeo177, 2008.

Peng, X., Wang, T., Wang, W., Ravishankara, A., George, C., Xia, M., Cai, M., Li, Q., Salvador, C. M., and Lau, C.: Photodissociation of particulate nitrate as a source of daytime tropospheric Cl_2, Nat. Commun., 13, 1-10, https://doi.org/10.1038/s41467-022-28383-9, 2022.

Peng, X., Wang, W., Xia, M., Chen, H., Ravishankara, A. R., Li, Q., Saiz-Lopez, A., Liu, P., Zhang, F., Zhang, C., Xue, L., Wang, X., George, C., Wang, J., Mu, Y., Chen, J., and Wang, T.: An unexpected large continental source of reactive bromine and chlorine with significant impact on wintertime air quality, Natl. Sci. Rev., 8, nwaa304, https://doi.org/10.1093/nsr/nwaa304, 2021.

Phillips, G. J., Tang, M. J., Thieser, J., Brickwedde, B., Schuster, G., Bohn, B., Lelieveld, J., and Crowley, J. N.: Significant concentrations of nitryl chloride observed in rural continental Europe associated with the influence of sea salt chloride and anthropogenic emissions, Geophys. Res. Lett., 39, L10811, https://doi.org/10.1029/2012gl051912, 2012.

Riedel, T. P., Bertram, T. H., Crisp, T. A., Williams, E. J., Lerner, B. M., Vlasenko, A., Li, S. M., Gilman, J., de Gouw, J., Bon, D. M., Wagner, N. L., Brown, S. S., and Thornton, J. A.: Nitryl chloride and molecular chlorine in the coastal marine boundary layer, Environ. Sci. Technol., 46, 10463-10470, https://doi.org/10.1021/es204632r, 2012.

Rutherford, J. A., Koehl, W. J., Benson, J. D., Burns, V. R., Hochhauser, A. M., Knepper, J. C., Leppard, W. R., Painter, L. J., Rapp, L. A., and Rippon, B.: Effects of Gasoline Properties on Emissions of Current and Future Vehicles-T50, T90, and Sulfur Effects-Auto/Oil Air Quality Improvement Research Program, SAE Technical Paper, 0148-7191, https://doi.org/10.4271/952510, 1995.

Sommariva, R., Hollis, L. D. J., Sherwen, T., Baker, A. R., Ball, S. M., Bandy, B. J., Bell, T. G., Chowdhury,

M. N., Cordell, R. L., Evans, M. J., Lee, J. D., Reed, C., Reeves, C. E., Roberts, J. M., Yang, M., and Monks, P. S.: Seasonal and geographical variability of nitryl chloride and its precursors in Northern Europe, Atmos. Sci. Lett., 19, e844, https://doi.org/10.1002/asl.844, 2018.

Tan, Z., Fuchs, H., Hofzumahaus, A., Bloss, W. J., Bohn, B., Cho, C., Hohaus, T., Holland, F., Lakshmisha, C., Liu, L., Monks, P. S., Novelli, A., Niether, D., Rohrer, F., Tillmann, R., Valkenburg, T. S. E., Vardhan, V., Kiendler-Scharr, A., Wahner, A., and Sommariva, R.: Seasonal variation in nitryl chloride and its relation to gas-phase precursors during the JULIAC campaign in Germany, Atmos. Chem. Phys., 22, 13137-13152, https://doi.org/10.5194/acp-22-13137-2022, 2022.

Thaler, R. D., Mielke, L. H., and Osthoff, H. D.: Quantification of nitryl chloride at part per trillion mixing ratios by thermal dissociation cavity ring-down spectroscopy, Anal. Chem., 83, 2761-2766, https://doi.org/10.1021/ac200055z, 2011.

Tham, Y. J., Wang, Z., Li, Q., Wang, W., Wang, X., Lu, K., Ma, N., Yan, C., Kecorius, S., Wiedensohler, A., Zhang, Y., and Wang, T.: Heterogeneous N_2O_5 uptake coefficient and production yield of $ClNO_2$ in polluted northern China: roles of aerosol water content and chemical composition, Atmos. Chem. Phys., 18, 13155-13171, https://doi.org/10.5194/acp-18-13155-2018, 2018.

Tham, Y. J., Wang, Z., Li, Q., Yun, H., Wang, W., Wang, X., Xue, L., Lu, K., Ma, N., Bohn, B., Li, X., Kecorius, S., Größ, J., Shao, M., Wiedensohler, A., Zhang, Y., and Wang, T.: Significant concentrations of nitryl chloride sustained in the morning: investigations of the causes and impacts on ozone production in a polluted region of northern China, Atmos. Chem. Phys., 16, 14959-14977, https://doi.org/10.5194/acp-16-14959-2016, 2016.

Thornton, J. A., Braban, C. F., and Abbatt, J. P.: N_2O_5 hydrolysis on sub-micron organic aerosols: the effect of relative humidity, particle phase, and particle size, Phys. Chem. Chem. Phys., 5, 4593-4603, https://doi.org/10.1039/B307498F, 2003.

Thornton, J. A., Kercher, J. P., Riedel, T. P., Wagner, N. L., Cozic, J., Holloway, J. S., Dubé, W. P., Wolfe, G. M., Quinn, P. K., Middlebrook, A. M., Alexander, B., and Brown, S. S.: A large atomic chlorine source inferred from mid-continental reactive nitrogen chemistry, Nature., 464, 271-274, https://doi.org/10.1038/nature08905, 2010.

Wahner, A., Mentel, T. F., Sohn, M., and Stier, J.: Heterogeneous reaction of N_2O_5 on sodium nitrate aerosol, J. Geophys. Res. Atmos., 103, 31103-31112, https://doi.org/10.1029/1998JD100022, 1998.

Wang, H., Yuan, B., Zheng, E., Zhang, X., Wang, J., Lu, K., Ye, C., Yang, L., Huang, S., and Hu, W.:

Formation and impacts of nitryl chloride in Pearl River Delta, Atmos. Chem. Phys., 22, 14837-14858, https://doi.org/10.5194/acp-22-14837-2022, 2022.

Wang, H., Wang, H., Lu, X., Lu, K., Zhang, L., Tham, Y. J., Shi, Z., Aikin, K., Fan, S., Brown, S. S., and Zhang, Y.: Increased night-time oxidation over China despite widespread decrease across the globe, Nat. Geosci., 16, 217-223, https://doi.org/10.1038/s41561-022-01122-x, 2023.

Wang, H., Chen, X., Lu, K., Tan, Z., Ma, X., Wu, Z., Li, X., Liu, Y., Shang, D., Wu, Y., Zeng, L., Hu, M., Schmitt, S., Kiendler-Scharr, A., Wahner, A., and Zhang, Y.: Wintertime N_2O_5 uptake coefficients over the North China Plain, Sci. Bull., 65, 765-774, https://doi.org/10.1016/j.scib.2020.02.006, 2020.

Wang, T., Tham, Y. J., Xue, L., Li, Q., Zha, Q., Wang, Z., Poon, S. C. N., Dubé, W. P., Blake, D. R., Louie, P. K. K., Luk, C. W. Y., Tsui, W., and Brown, S. S.: Observations of nitryl chloride and modeling its source and effect on ozone in the planetary boundary layer of southern China, J. Geophys. Res. Atmos., 121, 2476-2489, https://doi.org/10.1002/2015JD024556, 2016.

Xia, M., Peng, X., Wang, W., Yu, C., Wang, Z., Tham, Y. J., Chen, J., Chen, H., Mu, Y., and Zhang, C.: Winter $ClNO_2$ formation in the region of fresh anthropogenic emissions: seasonal variability and insights into daytime peaks in northern China, Atmos. Chem. Phys., 21, 15985-16000, https://doi.org/10.5194/acp-21-15985-2021, 2021.

Xia, M., Peng, X., Wang, W., Yu, C., Sun, P., Li, Y., Liu, Y. A. H. C. t. A.-P. O. A. C., Xu, Z., Wang, Z., Xu, Z., Nie, W., Ding, A., and Wang, T.: Significant production of $ClNO_2$ and possible source of Cl_2 from N_2O_5 uptake at a suburban site in eastern China, Atmos. Chem. Phys., 20, 6147-6158, https://doi.org/10.5194/acp-20-6147-2020, 2020.

Xue, L. K., Saunders, S. M., Wang, T., Gao, R., Wang, X. F., Zhang, Q. Z., and Wang, W. X.: Development of a chlorine chemistry module for the Master Chemical Mechanism, Geosci. Model Dev., 8, 3151-3162, https://doi.org/10.5194/gmd-8-3151-2015, 2015.

Yan, C., Tham, Y. J., Nie, W., Xia, M., Wang, H., Guo, Y., Ma, W., Zhan, J., Hua, C., and Li, Y.: Increasing contribution of nighttime nitrogen chemistry to wintertime haze formation in Beijing observed during COVID-19 lockdowns, Nat. Geosci., 16, 975-981, https://doi.org/10.1038/s41561-023-01285-1, 2023.

Yi, X., Sarwar, G., Bian, J., Huang, L., Li, Q., Jiang, S., Liu, H., Wang, Y., Chen, H., and Wang, T.: Significant Impact of Reactive Chlorine on Complex Air Pollution Over the Yangtze River Delta Region, China, J. Geophys. Res. Atmos., 128, e2023JD038898, https://doi.org/10.1029/2023JD038898, 2023.

Yun, H., Wang, T., Wang, W., Tham, Y. J., Li, Q., Wang, Z., and Poon, S. C. N.: Nighttime NO_x loss and

$ClNO_2$ formation in the residual layer of a polluted region: Insights from field measurements and an iterative box model, Sci. Total Environ., 622-623, 727-734, https://doi.org/10.1016/j.scitotenv.2017.11.352, 2018.

Zang, H., Zhao, Y., Huo, J., Zhao, Q., Fu, Q., Duan, Y., Shao, J., Huang, C., An, J., Xue, L., Li, Z., Li, C., and Xiao, H.: High atmospheric oxidation capacity drives wintertime nitrate pollution in the eastern Yangtze River Delta of China, Atmos. Chem. Phys., 22, 4355-4374, https://doi.org/10.5194/acp-22-4355-2022, 2022.

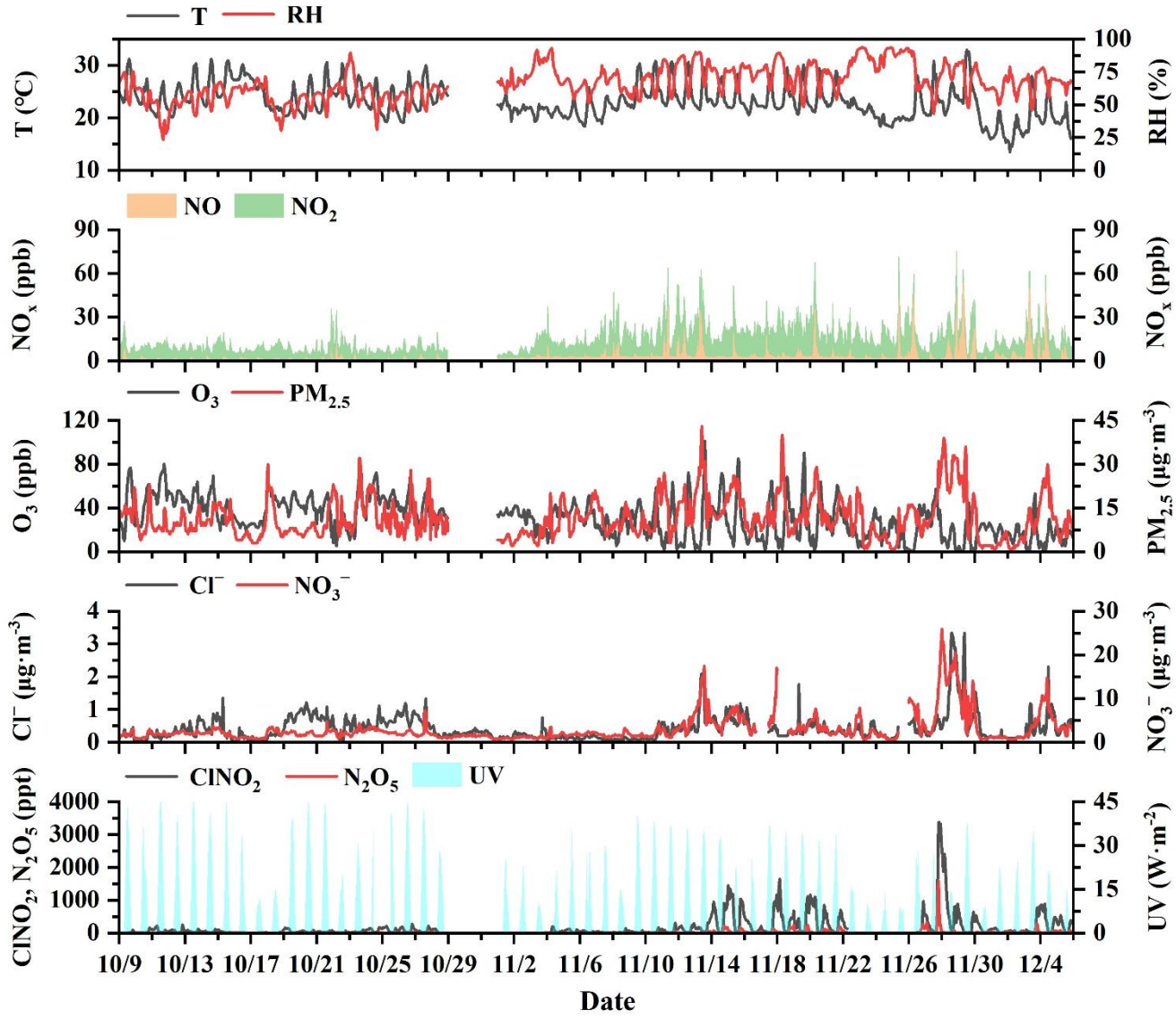

Figure 1. The time series of $ClNO_2$, related precursors, and meteorological parameters during the autumn observation period.

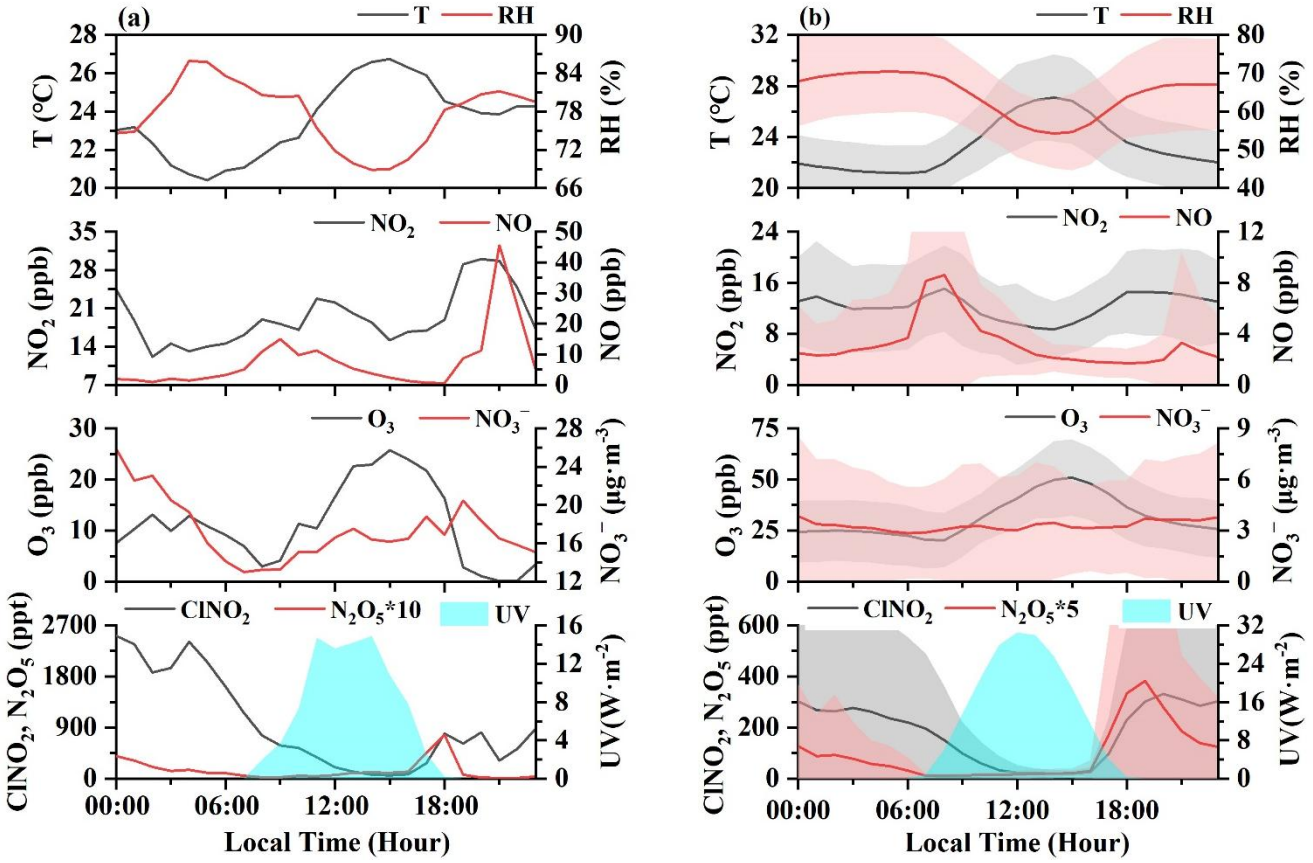

Figure 2. Diurnal variations of $ClNO_2$ and other related parameters for the highest concentrations of $ClNO_2$ (case) on November 28th (a) and the observation-average condition (from 9 October to 5 December) (b).

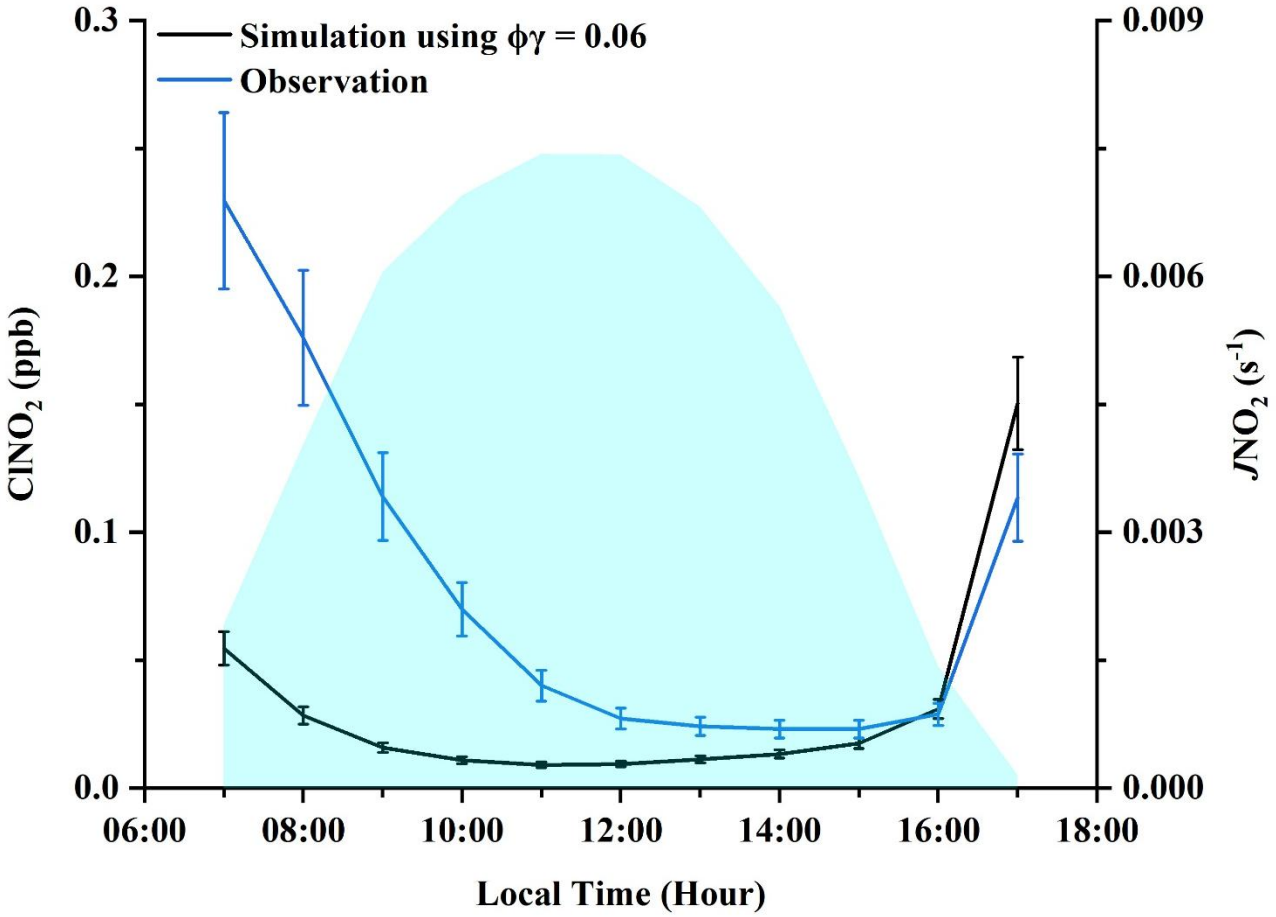

Figure 3. Comparisons of daytime $ClNO_2$ levels between observation and simulation with a $\phi(ClNO_2)$ of 1.0 and a $\gamma(N_2O_5)$ of 0.06 ($\phi\gamma = 0.06$).

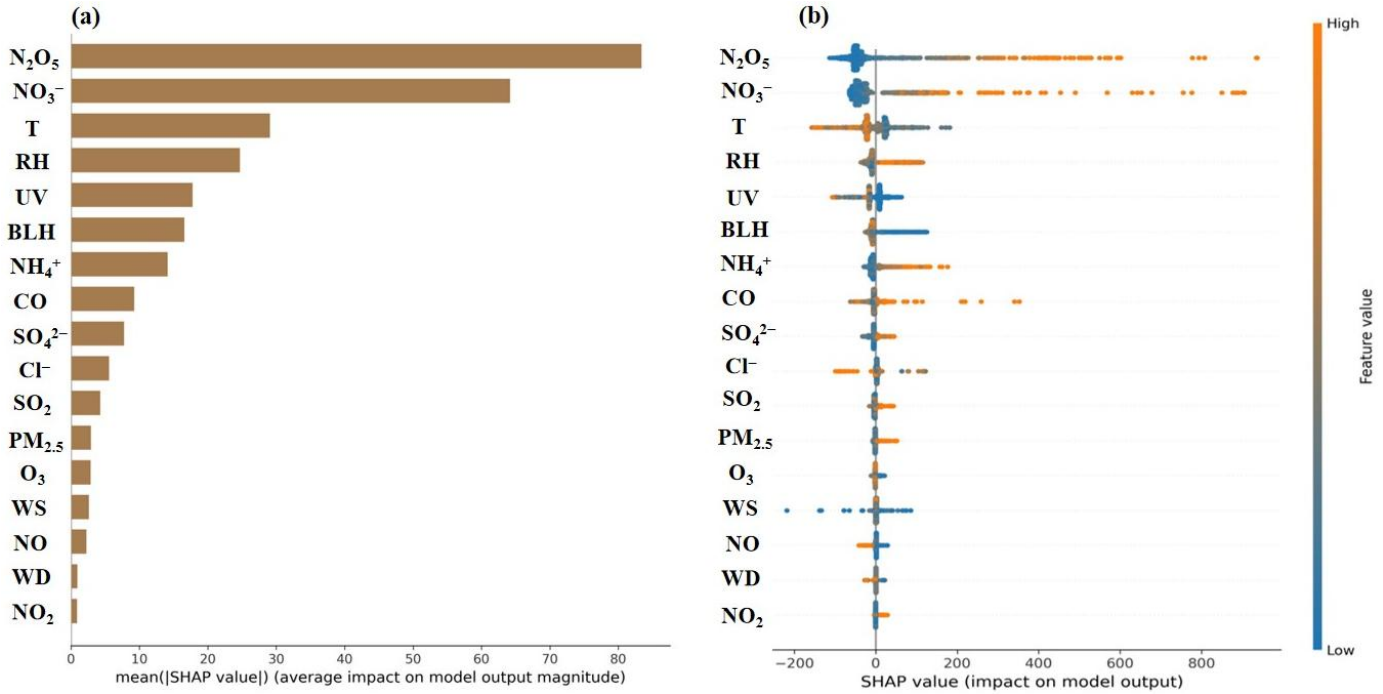

Figure 4. Relative importance of each feature to $ClNO_2$ using XGBoost-SHAP during the autumn observation period. The mean absolute SHAP value (a), summary plot of SHAP values of each feature (b).

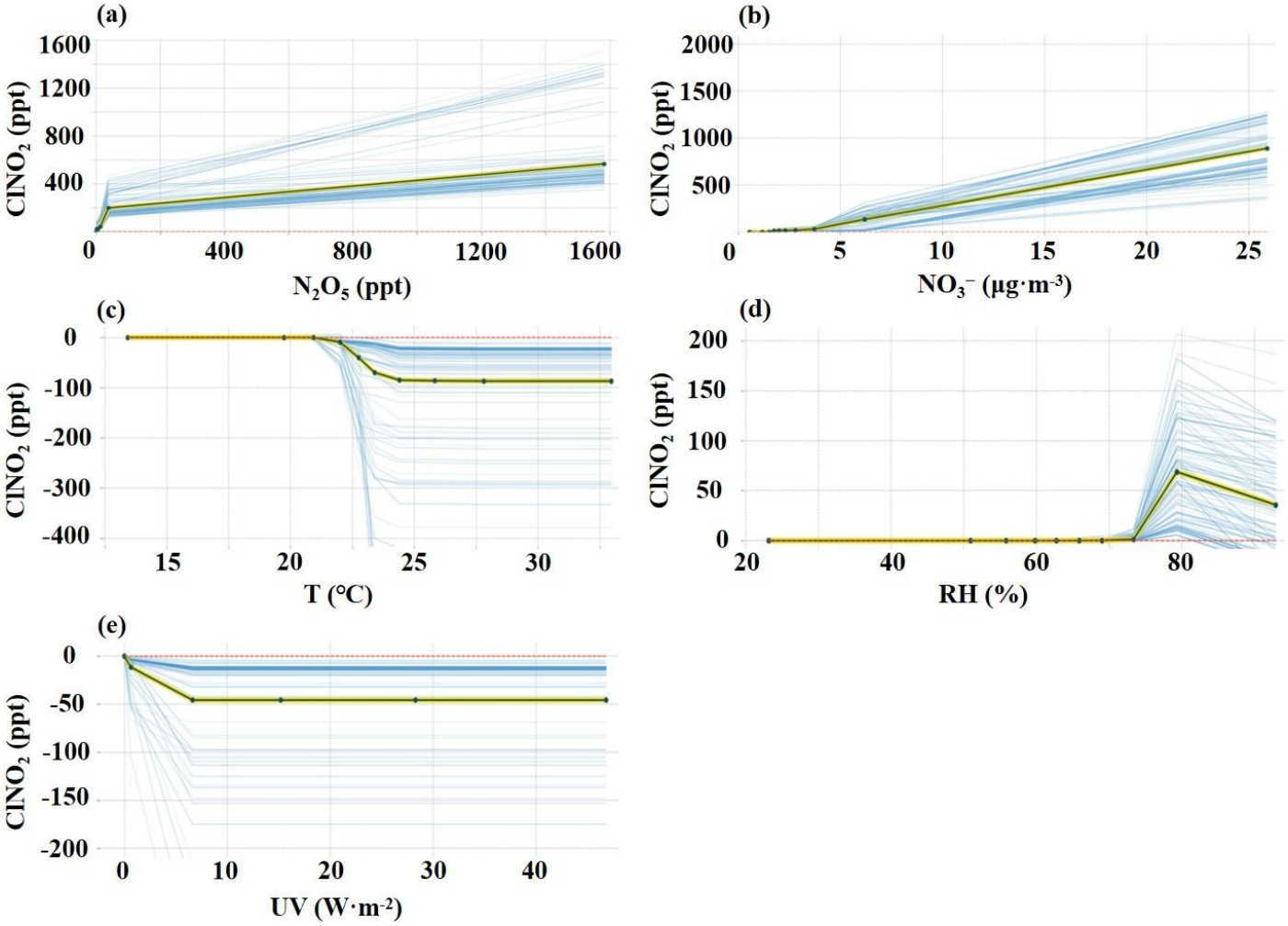

Figure 5. Isolation plots of PDP for N_2O_5 (a), NO_3^- (b), T (c), RH (d), and UV (e). The average variations of simulated $ClNO_2$ with factors' changes spline are indicated by the yellow and black curve, and blue curves presents all situations during the whole observation period.

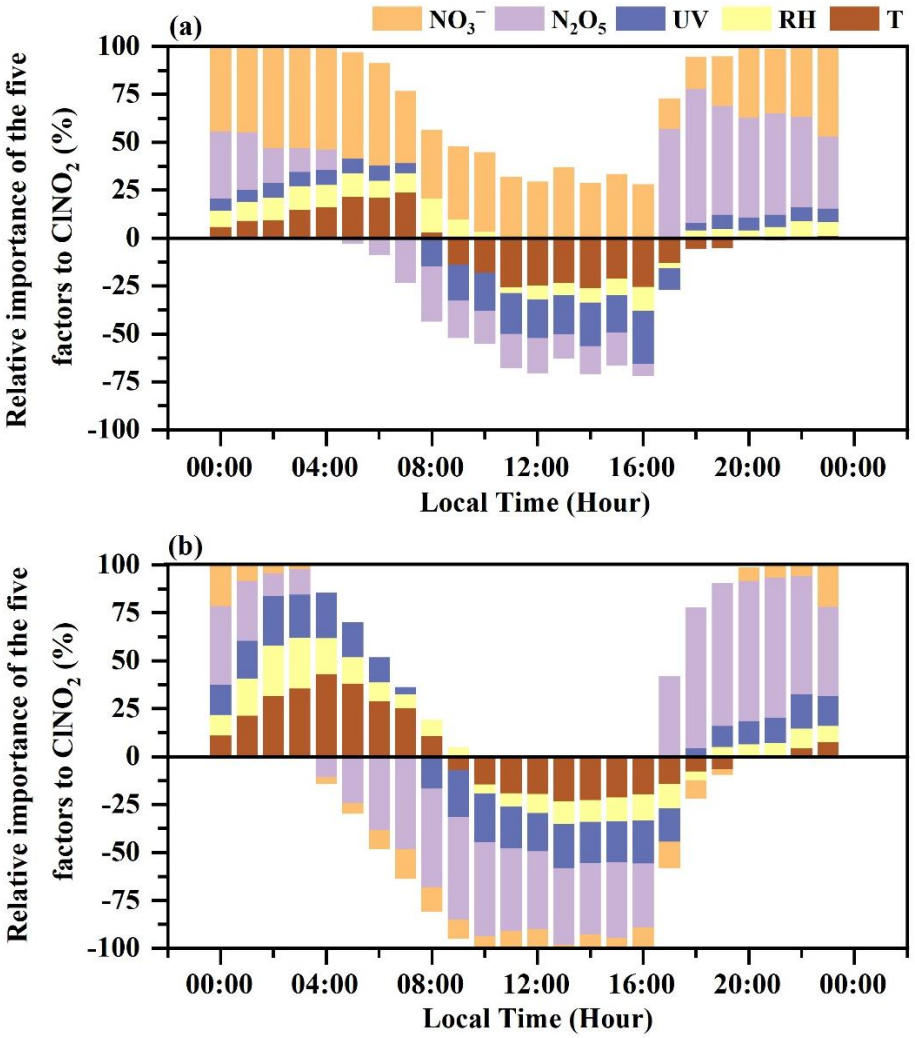

Figure 6. The diurnal variations of the relative importance of factors to $ClNO_2$ based on the SHAP values under the high (> 3.7 μg·m^{-3}) (a) and low (< 3.7 μg·m^{-3}) (b) $ClNO_2$ concentrations.

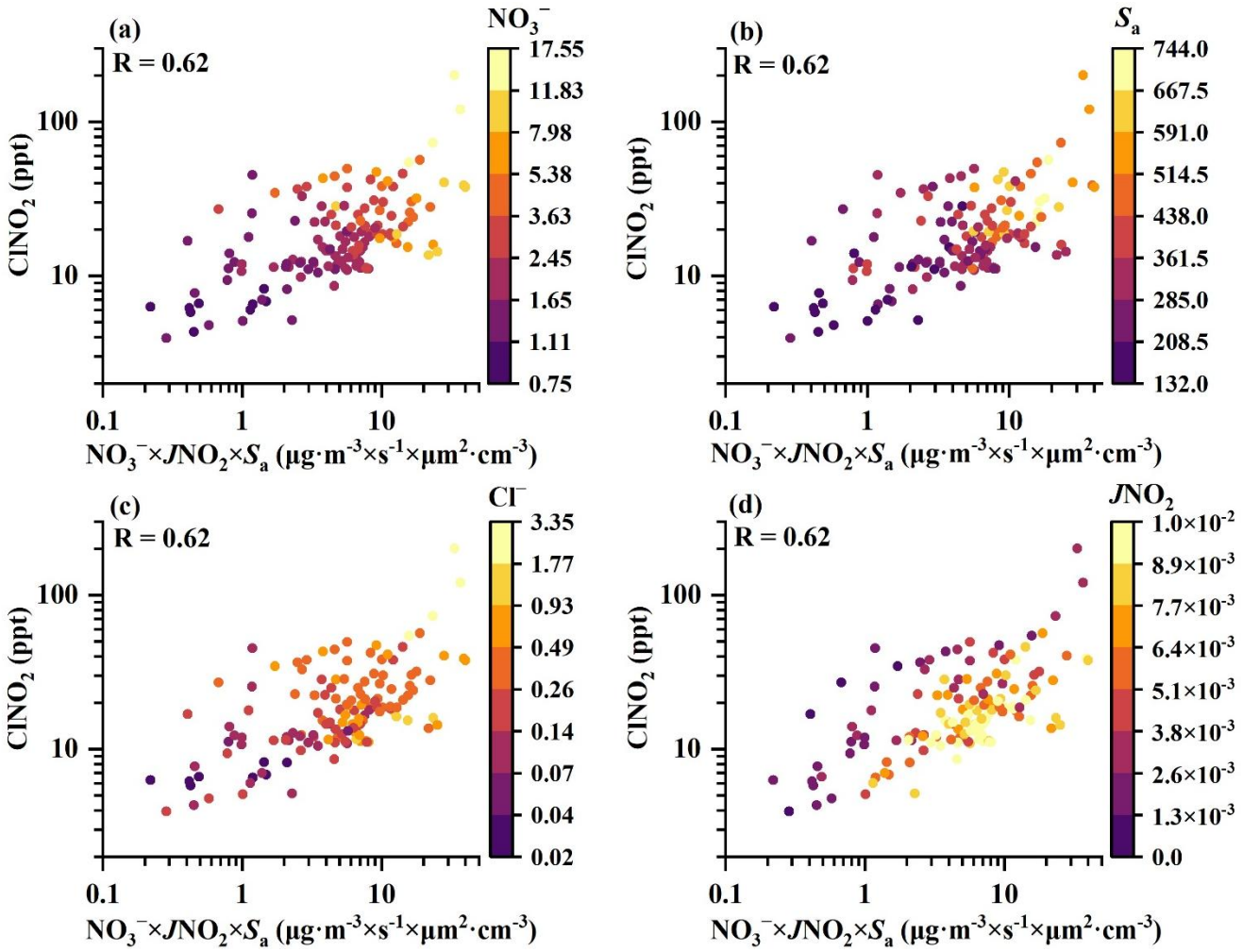

Figure 7. The relationship of daytime $ClNO_2$ concentrations (12:00-15:00 Local Time) and a proxy of nitrate (NO_3^-) photolysis (NO_3^-×JNO_2×S_a). The color of the dots respects the NO_3^- (a), S_a (b), Cl^- (c), JNO_2 (d), respectively.

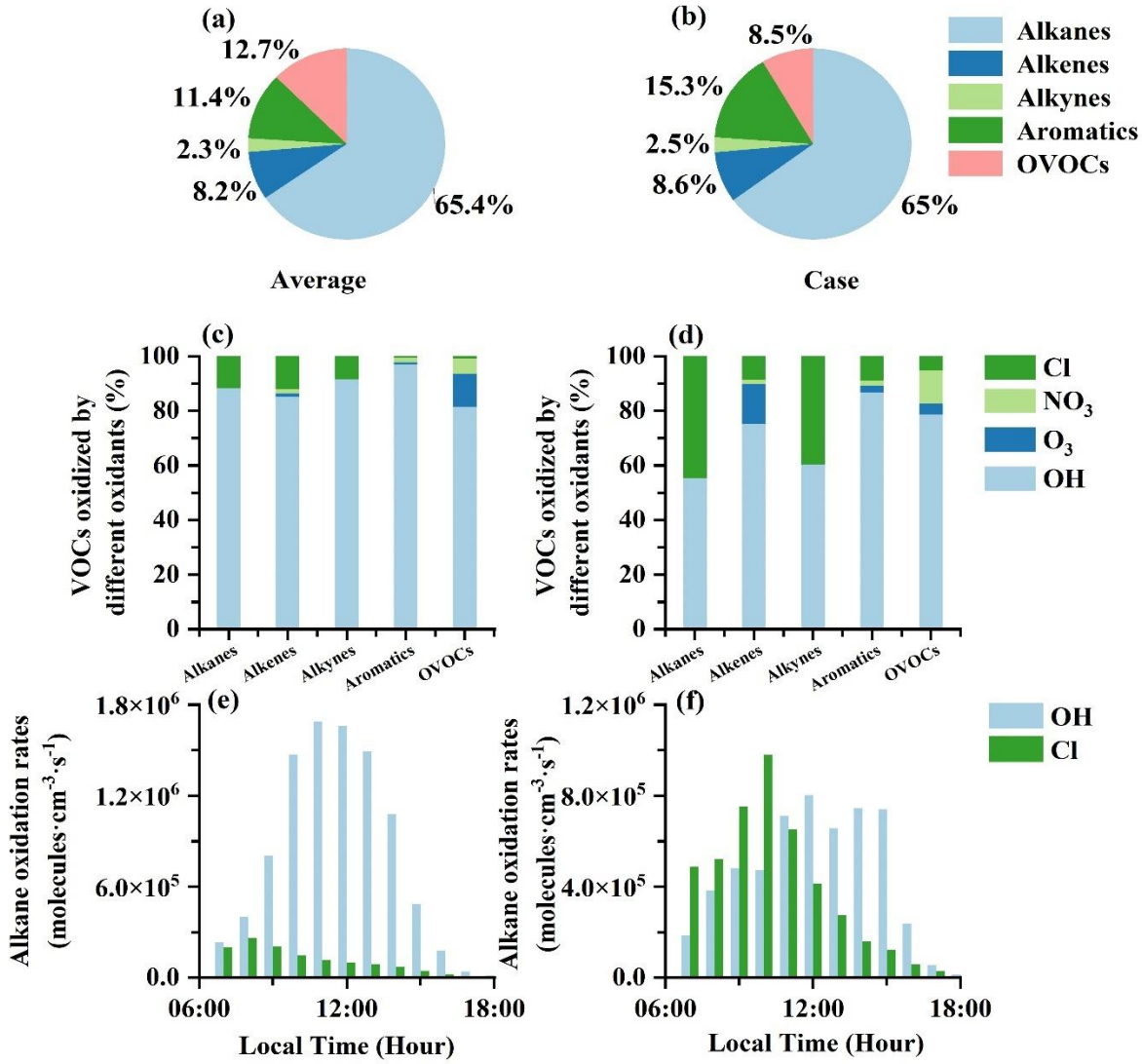

Figure 8. The impacts of Cl radials released by $ClNO_2$ photolysis and other atmospheric oxidants (including OH, NO_3, and O_3) on VOC oxidation under the observation-average condition and high $ClNO_2$ case, respectively. The contributions of different VOC groups oxidized by Cl radical during the observation-average (a). The contributions of different VOC groups oxidized by Cl radical during the case (b). The contributions of different atmospheric oxidants (including OH, Cl, NO_3, and O_3) to VOC groups during the observation-average (c). The contributions of different atmospheric oxidants (including OH, Cl, NO_3, and O_3) to VOC groups during the case (d). Comparisons of alkane oxidation rates (molecules·cm^{-3}·s^{-1}) by OH and Cl radical during the observation-average (e). Comparisons of alkane oxidation rates by OH and Cl radical (molecules·cm^{-3}·s^{-1}) during the case (f).

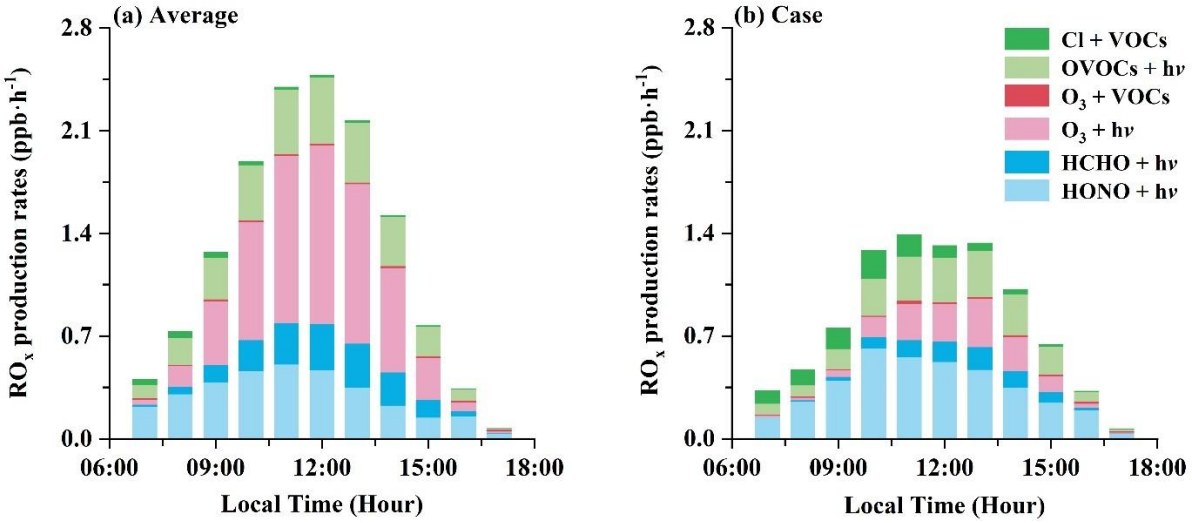

Figure 9. The contributions of different production pathways to RO_x production rates under the observation-average condition (a) and high $ClNO_2$ case (b), respectively.

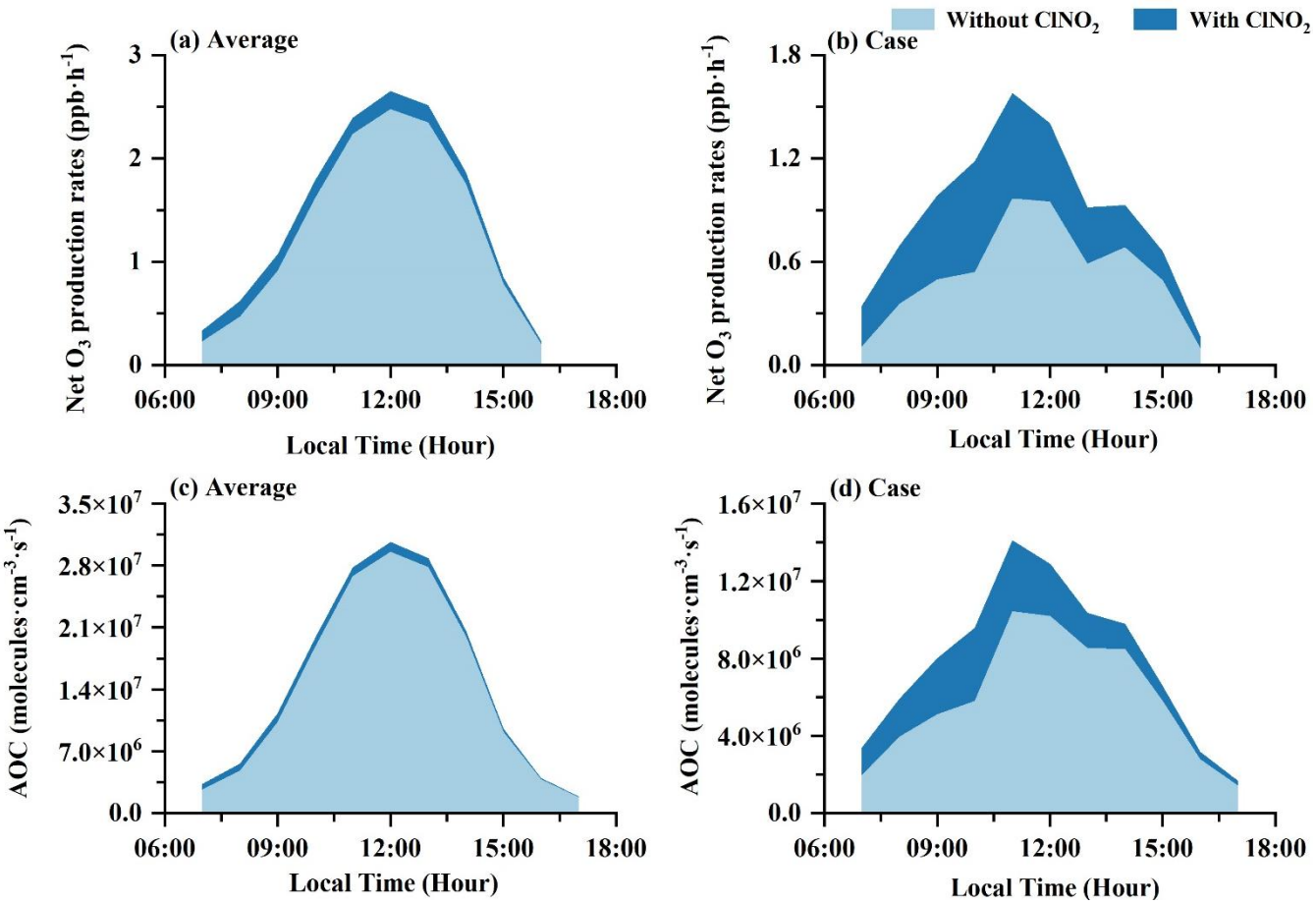

Figure 10. The impacts of Cl radials released by $ClNO_2$ photolysis on net O_3 production rates and the AOC levels under the observation-average condition (a, c) and high $ClNO_2$ case (b, d), respectively.

Table 1. Relative importance of Cl, OH, and O_3 to the daytime oxidation of VOC groups (including alkanes, alkenes, alkynes, aromatics, and OVOCs) around the world (Xue et al., 2015; Bannan et al., 2015; Bannan et al., 2017; Rutherford et al., 1995; Fraser et al., 1997).

	Xiamen (average)	Xiamen (case)	Hong Kong (max)	London (average)	Weybourne (average)	Boston	LA
Alkane Cl%	11.7	44.8	53.0	3.5	1.0	8.5	9.9
Alkane OH%	88.3	55.2	47.0	96.5	99.0	91.5	90.1
Alkane O_3%	-	-	-	-	-	-	-
Alkene Cl%	12.2	8.7	14.0	0.6	0.4	0.3	0.3
Alkene OH%	85.0	75.2	81.0	77.9	78.3	33	31.3
Alkene O_3%	1.2	14.7	5.0	21.5	21.4	66.7	68.4
Alkyne Cl%	8.5	40.0	-	7.0	2.6	8.7	8.7
Alkyne OH%	91.5	60.0	-	91.8	96.7	89.7	89.7
Alkyne O_3%	-	-	-	1.2	0.7	1.6	1.6
Aromatics Cl%	0.7	9.1	11.0	-	-	-	-
Aromatics OH%	97.0	86.6	89.0	-	-	-	-
Aromatics O_3%	0.7	2.6	-	-	-	-	-
OVOCs Cl%	0.9	5.2	6.0	-	-	-	-
OVOCs OH%	81.4	78.7	85.0	-	-	-	-
OVOCs O_3%	12.0	3.9	-	-	-	-	-

693

694 Table 2. The impacts of $ClNO_2$ photolysis on RO_x (OH, HO_2, and RO_2) levels, $P(RO_x)$, and $P(O_3)$ around the
695 world (Xia et al., 2021; Wang et al., 2022; Tham et al., 2016; Wang et al., 2016; Xue et al., 2015; Bannan et
696 al., 2017; Jeong et al., 2019).

Study Area	Season	OH	HO_2	RO_2	$P(RO_x)$	$P(O_3)$
Xiamen (average)	Autumn	3.7%	7.1%	10.3%	4.9%	6.7%
Xiamen (case)	Autumn	17.9%	34.6%	54.3%	23.8%	41.7%
Wangdu/Beijing/Mt. Tai	Winter	15.0%–22.0%	24.0%–31.0%	36.0%–52.0%	1.3%–3.8%	1.3%–6.2%
Heshan	Autumn	1.5%–2.6%	1.9%–4.6%	3.0%–6.8%	< 2.2%	1.0%–4.9%
Wangdu	Summer	-	-	-	10%–30%	3.0%–13.0%
Mt. Tai Mo Shan, Hong Kong	Winter	40.0%–77.0%	53.0%–106.0%	-	-	11.0%–41.0%
Hok Tsui, Hong Kong	Summer	6.6%	12.2%	45.1%	-	10.3%
Weybourne	Spring	5.0%	7.0%	9.0%	-	-
Seoul	Spring	-	-	-	-	1.0%–2.0%

697